Mechano-self-regulation of bacterial size in growing colonies

René Wittmann,[1, *] G. H. Philipp Nguyen,[1] Hartmut Löwen,[1] Anupam Sengupta,[2, †] and Fabian J. Schwarzendahl[1, ‡]

[1]*Institut für Theoretische Physik II: Weiche Materie,*
Heinrich-Heine-Universität Düsseldorf, Universitätsstraße 1, 40225 Düsseldorf, Germany
[2]*Physics of Living Matter, Department of Physics and Materials Science,*
University of Luxembourg, 162 A, Avenue de la Faïencerie, L-1511 Luxembourg City, Luxembourg
(Dated: December 21, 2022)

We demonstrate that biomechanical forcing plays an important role as the driving force behind the dynamical self-regulation of cell size (or length) in growing bacterial colonies. In our experiments, the measured elongation rate decreases over time and depends on the areal packing density around each cell. To describe this phenomenon theoretically, we devise a cell-resolved model which includes as its key ingredient a force opposed to the growth process, accounting for mechano-self-regulation. Our model is analyzed analytically by a coarse-grained dynamical density functional theory and solved by cell-based computer simulations to predict how the strength of mechano-self-regulation depends on the bacterial size, the location in the colony and the local environment. The microscopic nature of this approach allows to quantify the effect of biomechanical interactions on the structure, composition and dynamical features of growing bacterial colonies.

Assemblies of rodlike particles can exhibit a large variety of intriguing collective ordering phenomena due to their internal orientational degrees of freedom — both in and out of equilibrium [1–7]. Specifically, over the last years, there has been an increasing interest in the biophysical properties of bacterial colonies expanding on nutrient-replete surfaces [8–10]. These colonies typically consist of rod-like agents whose size increases and which eventually divide in the course of a cell cycle [11–14]. The mechanical interactions between these bacteria have been identified as a key ingredient to determine the structure and shape of the growing colony [15–18]. Moreover, growing bacterial colonies have been recently reported to collectively self-regulate phenotypic traits over time [19]. Yet, how collective interactions at the scale of the colony enable bacterial populations to dynamically tune the size of single cells remains unknown. In particular, there is still a need for quantifying the effect of biomechanical forces between individual bacteria on the growth process, in view of the emerging *phenotemporal* behavior, i.e., the time-dependent distribution of bacterial sizes (or lengths), in course of the evolution of the growing colony [20].

Inspired by experiments, here we put forward a microscopic first-principles model derived from dynamical density functional theory (DDFT) [21–23] to predict the self-regulation of phenotemporal properties in a growing bacterial colony through a cell-length-resolved density [24, 25]. As compiled in Fig. 1, our model is designed to capture the fundamental aspects of bacterial growth (details on our methods and results are provided as supplementary information [26]). In our experiments, shown in the top panel of Fig. 1, we observe the growth of *Escherichia coli* at 30° C, on a nutrient-rich agarose

substrate. A single cell first divides into two cells of equal length which then continue to grow with a certain elongation rate. At later times, as the colony becomes denser, growth and cell division progress with reduced elongation rate. This effect is significantly more pronounced for closely packed cells in direct contact with their neighbors than for the loosely packed cells flanked by void regions of the colony. Overall, we observe that the average cell elongation rate is nearly halved in the grown colony.

As demonstrated by means of cell-resolved Langevin simulations in two dimensions, shown in the bottom panel of Fig. 1, the central experimental observations are modeled by accounting for four basic ingredients: division of a bacterium with length $2L$ into two shorter agents of length-at-birth L, growth with a certain elongation rate, fluctuations of the elongation rate and mechano-self-regulation. By the latter, we denote a mechanical force which reflects the ability of the individual bacteria to sense the presence of other bacteria in their surrounding (or external stimuli) [27, 28] and, based on this information, self-regulate their growth behavior to avoid overcrowding [29]. As the main prediction of this model, we observe in Fig. 1Q an effective reduction of the bacterial elongation rate over time. Specifically, our length-resolved DDFT provides analytic insight into the growth process, predicting the evolution towards a unique distribution of cell lengths, which reflects the stochastic nature of growth. On top, our cell-based simulations reveal the spatiotemporal aspects of mechano-self regulation.

In the spirit of DDFT, we describe the growth dynamics of the bacterial colony by its density $\rho(l, t)$ explicitly resolving the size of the bacteria, represented here by a length l. Having reached the maximal length $l = 2L$, each bacterium splits into two new individuals with length-at-birth L. To make analytic progress, we restrict l to the interval $l \in [L, 2L]$ and incorporate cell division through the oblique boundary condition

$$\rho(L, t) = 2\rho(2L, t) . \tag{1}$$

* rene.wittmann@hhu.de
† anupam.sengupta@uni.lu
‡ fabian.schwarzendahl@hhu.de

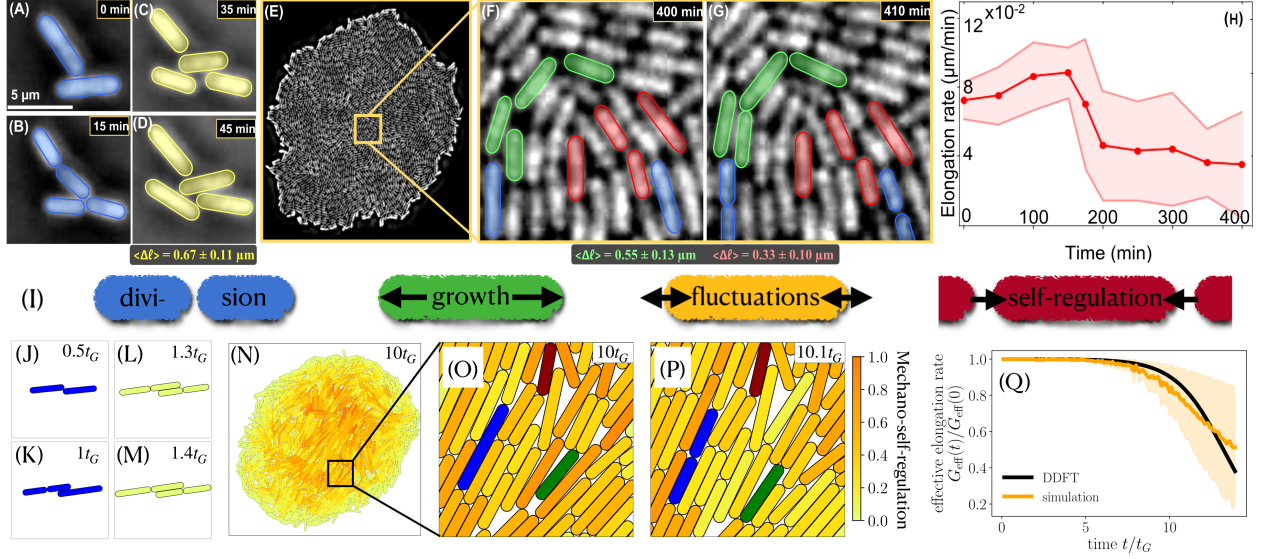FIG. 1. Decreasing bacterial elongation rate in a growing colony. **Top:** Experiments on a monolayer of cells dividing every ∼30 minutes on a nutrient-rich agarose substrate, reaching a cell count of ∼4500 bacteria after 450 minutes. (A, B) Division of cells (hued in blue) in the early stage of the colony. (C, D) Growth of cells (hued in yellow) during the early phase over an interval of 10 minutes. The average cell elongation rate $\langle \Delta l \rangle/10$min is 0.067 ± 0.011 μm/min. (E) Micrograph of a well-developed bacterial monolayer comprising about 2600 cells. (F, G) Division of cells (hued in blue) and growth of both loosely and densely packed cells (hued in green and red) over an interval of 10 minutes within the dense colony. The corresponding average elongation rates are 0.055 ± 0.013 μm/min and 0.033 ± 0.01 μm/min, respectively. (H) Cell elongation rate of all bacteria as a function of time. **Bottom:** Corresponding predictions of our theoretical model (I), where $t_G := L/G$ is the time between the first two divisions. (J-P) Simulation snapshots reflecting the experimental images shown above with the strength of the mechanical interactions on each bacterium highlighted by color. In the closeups (O,P) of the dense colony, we also highlight selected cells showing division (blue), fast growth in a dilute region (green) and slow growth in a dense region (red). (Q) Effective elongation rate $G_{\text{eff}}(t)$, defined in Eq. (5), from DDFT using the analytic result of Eq. (4) and simulation (6) with numerical errors for the fluctuation parameter $D = 10^{-2}GL$. The parameters $S = 10^{-4}G/\bar{\rho}_0$ and $\tilde{S} = 5 \times 10^3 G/L^{3/2}$ for mechano-self-regulation are chosen to obtain a comparable decay behavior.

The total density $\rho(l, t) \equiv \bar{\rho}(t) \, h(l, t)$, can be conveniently expressed by the normalized length distribution $h(l, t)$ with $\int dl \, h(l, t) = 1$ and the length-averaged density $\bar{\rho}(t)$.

In our model the colony's time evolution is given by

$$\partial_t \rho(l, t) = \partial_l \big(-G\rho(l, t) + D\partial_l \rho(l, t) + S\rho(l, t)\bar{\rho}(t) \big), \quad (2)$$

where ∂_i is short for the partial derivative with respect to $i = t, l$. The first term in the brackets is a constant drift term which describes the bacterial growth with (average) elongation rate G, driving the system out of equilibrium. The second term is of diffusive nature and models elongation-rate fluctuations with magnitude D. Finally, the last term in Eq. (2) represents the mechanical interactions of strength S. Here, we use a mean-field description for soft interactions in the form of Gaussian cores [30], but also more general interactions can be incorporated through appropriate free-energy functionals [31–34].

The phenotemporal description of $\rho(l, t)$ in Eq. (2) can be thought of as a coarse-grained model after integrating out positions and orientations of a more general DDFT [26]. In turn, if one is only interested in the increase of the density $\bar{\rho}(t)$, we recover after further coarse graining

the bare growth equation

$$\partial_t \bar{\rho}(t) = \bar{\rho}(t) \left(R - \frac{S \ln 2}{L} \bar{\rho}(t) \right) \quad (3)$$

reminiscent of models for (space-resolved) population dynamics [35, 36]. In connection with Eq. (2) we identify the overall growth rate $R = G \ln(2)/L + D(\ln(2)/L)^2$.

As one of our main results, mechano-self regulation ($S > 0$) slows down the growth and the colony eventually attains a stationary state. Specifically, solving Eq. (3) with $\bar{\rho}_0 := \bar{\rho}(0)$ we find that the average density

$$\bar{\rho}(t) = \frac{R\bar{\rho}_0}{\frac{S \ln 2}{L} \bar{\rho}_0 + (R - \frac{S \ln 2}{L} \bar{\rho}_0)e^{-Rt}}, \quad (4)$$

approaches the maximal value $\bar{\rho}(\infty) = \frac{RL}{S \ln 2}$ for $t \to \infty$. From Eq. (4), we then find the effective elongation rate

$$G_{\text{eff}}(t) := G + D\frac{\ln 2}{L} - S\bar{\rho}(t), \quad (5)$$

shown in Fig. 1Q, which decays to zero when all available space is occupied for $t \to \infty$. These results serve as a reference for the solutions of Eq. (2) for nonuniform
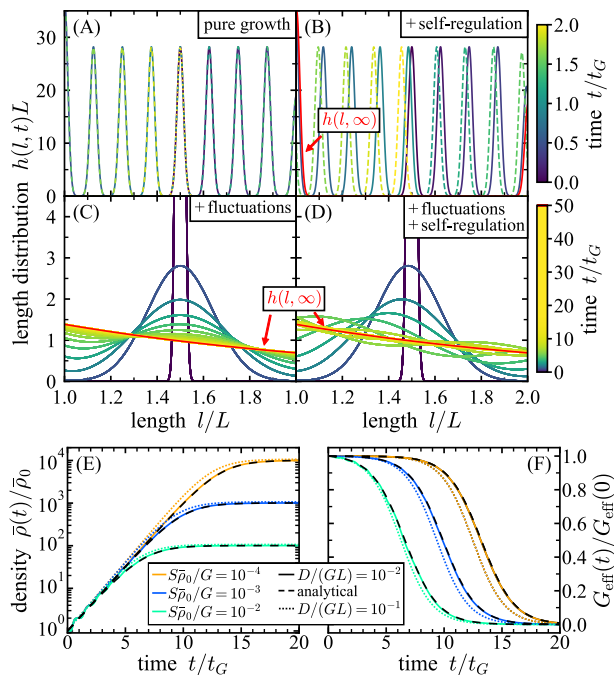
FIG. 2. DDFT results from Eq. (2) with Eq. (1). (A-D) Time evolution (color bar) of the length distribution from an initial Gaussian peak centered at $l = L/2$ with parameters $S = 0$ (left) or $S = 10^{-2}G/\bar{\rho}_0$ (right) and $D = 0$ (top) or $D = 10^{-2}GL$ (bottom). If a stationary distribution $h(l,\infty)$ exists, it is drawn in red. (E,F) Time evolution of the average density $\bar{\rho}(t)$ and the effective elongation rate $G_{\text{eff}}(t)$ for different parameters (as labeled). The respective analytic predictions of Eqs. (4) and (5) are drawn as black dashed lines.
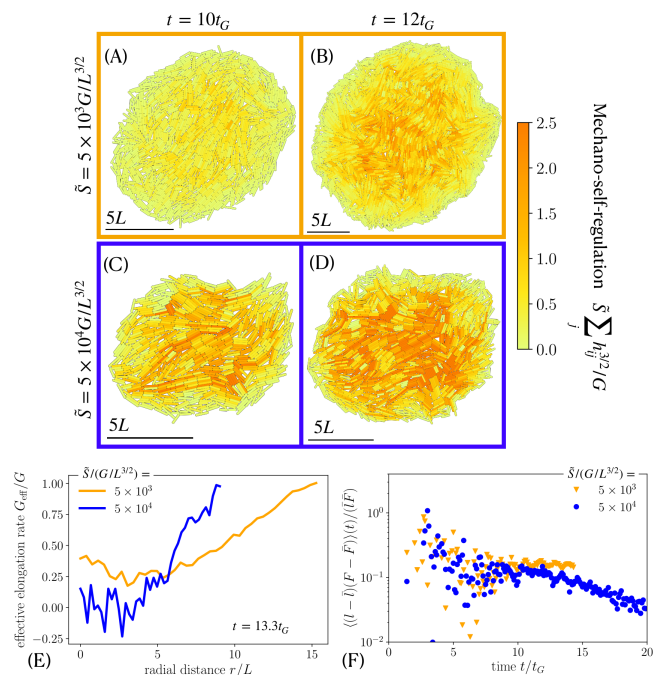

FIG. 3. Cell-based simulation results from Eq. (6). (A-D) Snapshots as in Fig. 1N (different color bar) of two colonies with $D = 10^{-2}GL$ but different mechano-self-regulation $\bar{S}$ at two times (see annotations). (E) Local effective elongation rate as a function of the radial distance r from the colony center of mass. (F) Normalized length-force correlation.

length distribution $h(l,t)$, e.g., when initializing $h_0(l) := h(l,0)$ with a peak to represent a single bacterium.

Together with the boundary condition (1), our phenotemporal DDFT (2) provides valuable analytic insight into the growth process [26], as compiled in Fig. 2. In the absence of both fluctuations ($D = 0$) and interactions ($S = 0$), we observe an *oscillating growth*, cf. Fig. 2A, where $h(l,t) \propto 2h_0(l+\Delta l(t))+h_0(l+\Delta l(t)-L)$ is periodic in time as the horizontal offset $\Delta l(t)$ increases linearly from 0 to L within one period $t_G := L/G$, which sets out time unit. After each generation, denoted by an integer n such that $\Delta l(t = nt_G) = 0$, the distribution resorts to its initial form $h_0(l) := h(l,0)$ and the average density $\bar{\rho}(nL/G) = 2^n \bar{\rho}_0$ has doubled. With interactions ($S > 0$ but $D = 0$), we observe a *retarded growth*, cf. Fig. 2B, where the period of these oscillations increases from generation to generation, as the effective elongation rate (5) decreases over time. When the density $\bar{\rho}(\infty) = G/S$ reaches its stationary value in course of the birth of a new generation, the length distribution is suddenly arrested. With fluctuations ($D > 0$ but $S = 0$), we observe *uniform growth*, cf. Fig. 2C, where the distribution broadens and approaches the unique limit $h(l,\infty) \propto 2^{-l/L}$, without setting a limit to the indefinite exponential growth of $\bar{\rho}(t)$. For extreme fluctuations ($D \gg S$ and $D \gg G/\bar{\rho}_0$) our

model predicts a *fluctuation-driven growth* (not shown) with $h(l,\infty) \propto (3L - l)$.

Combining the behavior from the above special cases, the full dynamics in Eq. (2) can be understood as *retarded and uniform growth*, cf. Fig. 2D, where the distribution $h(l,t)$ simultaneously broadens and increases its period in the course of time. Hence, the average density $\bar{\rho}(t)$ increases jerkily due to correlated division bursts, as shown in Fig. 2E. The coarse-grained prediction from Eq. (4) is recovered after a certain time when the length distribution has approached $h(l,\infty) \propto 2^{-l/L}$ due to fluctuations. Another consequence of a nonuniform length distribution is an effective elongation rate which depends on the instantaneous length distribution [26]. For the average effective elongation rate $G_{\text{eff}}(t)$, defined in Eq. (5), we observe in Fig. 2F an earlier decay for both increasing mechano-self regulation (stronger counter-force) and increasing fluctuations (faster growth). Moreover, $G_{\text{eff}}(t)$ shows a jerky behavior for weak fluctuations, just like the average density.

To corroborate the predictions of our probabilistic DDFT and gain further insight, we perform cell-resolved Langevin simulations of the spatio- and phenotemporal growth process locally limited by mechano-self regulation [26]. To this end, we consider rod-like bacteria of lengths l_i which interact through Hertzian repulsion and couple the Langevin equations for positions and orienta-

tions to the stochastic length dynamics

$$\partial_t l_i = G + \sqrt{2D}\xi_i + \tilde{S}\sum_j h_{ij}^{3/2}\,, \qquad (6)$$

where h_{ij} is the overlap of two cells i, j and ξ_i a white noise of unit variance. Due to the different nature of interactions considered the mechano-self-regulation parameter $\tilde{S}$ is different from S in Eq. (2).

The effective elongation rate $G_{\rm eff}(t)$ averaged over the whole colony is shown in Fig. 1Q. As in the experiment $G_{\rm eff}(t)$ decreases at later times but does not rapidly approach zero since the continuously growing periphery of the colony always remains sufficiently dilute. Our local simulation results compiled in Fig. 3 reveal that the mechanical force on longer bacteria is typically stronger than on shorter bacteria and that the local elongation rate increases from the colony center to the periphery. For a stronger overall mechano-self regulation (larger $\tilde{S}$), the colony grows slower and the difference between the typical forces in these two regions is more significant. Moreover, as illustrated in Fig. 1O to P, the local force acting on a bacterium in a dense colony is smaller when it is surrounded by voids than when it is in close contact with its neighbors, which also feeds back on the individual elongation rate measured in our experiment, cf. Fig. 1F to G.

To gain further insight into the length-distribution dynamics, we compare in Fig. 4 the experimental results for the average length $\bar{l}(t) := \int {\rm d}l\, l\, h(l, t)$ and the normalized variance $\Delta(t) := \int {\rm d}l\, (l - \bar{l}(t))^2\, h(l,t)/(\bar{l}(t))^2$ to our model predictions. After early fluctuations owed to the synchronous cell cycles in the early generations, the experimental data show a clear trend that the bacteria become shorter in the dense colony, while the variance begins to plateau under the experimental growth conditions considered here. The moments from DDFT oscillate around their values for the uniform distribution $h(l, \infty) \propto 2^{-l/L}$. The experimental observations are even better captured by a refined DDFT, modeling cell division through source and sink terms and replacing Eq. (1) with a directed condition that prevents flow through the boundary from short to long [26]. This predicts the expected decrease of $\bar{l}(t)$ when the colony has grown sufficiently dense. We find similar results from cell-based simulations, where some bacteria in the dense region self-regulate their length below the length-at-birth L.

We have introduced a DDFT model for growing bacterial colonies from which we predicted analytical length distributions and drew parallels to dynamical observations in experiments and Langevin simulations. Our description of mechano-self regulation both contributes to a comprehensive theoretical understanding of growing bacterial colonies and elucidates the role of biomechanical forces in living samples. One possible application of our mechanical self-regulating force is to explain the onset of the mono-to-multilayer transition (or verticalization) [10, 19, 37], i.e., when individual bacteria evade crowded regions by escaping into the third dimension to
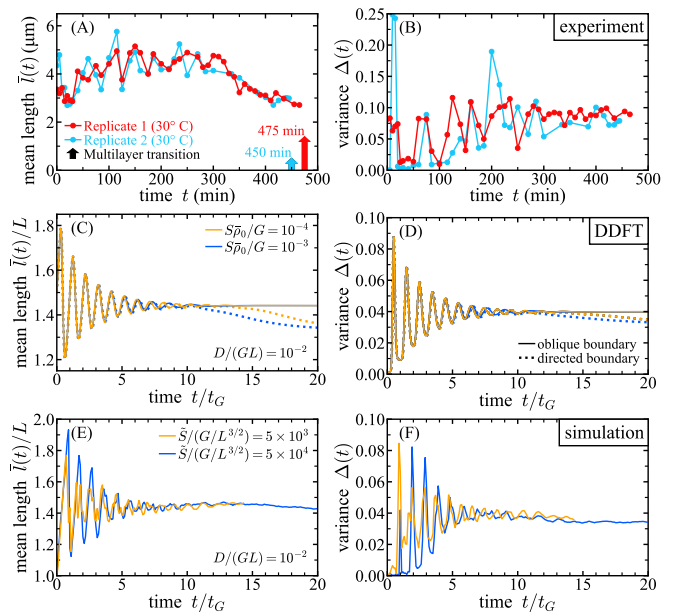

FIG. 4. Time dependent moments of the length distribution. We compare the average cell length $\bar{l}(t)$ (left) and the normalized variance $\Delta(t)$ of the cell length (right) for two biological replicates in the experiment (top) until the mono-to-multilayer transition [10] (upward arrows). We also show our model predictions using DDFT with an oblique boundary (1) and a refined version with a directed boundary condition [26] (middle) and cell-based simulations (bottom) with comparable parameters, cf. Fig. 1Q, as labeled.

form new layers. In our experiments this happens after about 450 minutes, which roughly corresponds to $t \approx 13 t_G$ for the model parameters chosen accordingly in Fig. 1Q. Our model intuitively suggests that this transition occurs when the local in-plane mechanical force opposing the growth, as measured in Fig. 3A to D, exceeds a certain threshold.

To provide a broader account of biodiversity and internal cell processes in future work, our model can be readily extended by considering a self-regulated life time or length-at-birth [13, 14], nonlinear cell elongation [19, 38, 39], death events [40, 41] or division into multiple daughter cells [42], as well as to describe multiple species of bacteria with different properties [43, 44], including phenotype switching [45, 46] or mutation [16, 47, 48]. A logical extension of our DDFT is to additionally resolve positions and orientations [33, 34, 49]. Both this generalized DDFT [26] and our cell-based simulations allow to explore the spatiotemporal effects of a heterogeneous local length distribution when investigating the colony structure [41, 50–52], interactions between multiple colonies [53–55], confinement effects [56–58], topological defect dynamics [19, 59–63], emerging smectic order [18, 64–68] or growth into the third dimension [19, 37, 69, 70]. Attractions through pili bonds [53, 54], or the capability of individual bacteria to enter a motile state [71, 72] can also be modeled. Moreover, it will be

interesting to study growth within porous media [73, 74] or to include other spatially distributed agents interacting with the growing colony, such as nutrients [75, 76], antibiotics [43, 77], parasites like bacteriophages [78] or a secreted extracellular matrix mediating biofilm formation [52, 75]. Finally, our DDFT equations allow for a systematic derivation [79, 80] of phase-field crystal models [81] to recover hydrodynamic field equations [9, 60, 61] and explicitly incorporate aspects related to bacterial length. Exploring the relation to active nematics [82] constitutes an interesting perspective.

[1] T. Vicsek and A. Zafeiris, Phys. Rep. **517**, 71 (2012).
[2] M. Bär, R. Großmann, S. Heidenreich, and F. Peruani, Annu. Rev. Condens. Matter Phys. **11**, 441 (2020).
[3] P. Kraikivski, R. Lipowsky, and J. Kierfeld, Phys. Rev. Lett. **96**, 258103 (2006).
[4] V. Narayan, S. Ramaswamy, and N. Menon, Science **317**, 105 (2007).
[5] A. Díaz-De Armas, M. Maza-Cuello, Y. Martínez-Ratón, and E. Velasco, Phys. Rev. Res. **2**, 033436 (2020).
[6] N. Kumar, R. K. Gupta, H. Soni, S. Ramaswamy, and A. K. Sood, Phys. Rev. E **99**, 032605 (2019).
[7] T. Kozhukhov and T. N. Shendruk, Sci. Adv. **8**, eabo5788 (2022).
[8] R. J. Allen and B. Waclaw, Rep. Prog. Phys. **82**, 016601 (2018).
[9] Z. You, D. J. G. Pearce, A. Sengupta, and L. Giomi, Phys. Rev. X **8**, 031065 (2018).
[10] Z. You, D. J. G. Pearce, A. Sengupta, and L. Giomi, Phys. Rev. Lett. **123**, 178001 (2019).
[11] A. N. Malmi-Kakkada, X. Li, H. S. Samanta, S. Sinha, and D. Thirumalai, Phys. Rev. X **8**, 021025 (2018).
[12] M. Banwarth-Kuhn, J. Collignon, and S. Sindi, Applied Sciences **10**, 5780 (2020).
[13] J. Li, S. K. Schnyder, M. S. Turner, and R. Yamamoto, Phys. Rev. X **11**, 031025 (2021).
[14] A. Colin, G. Micali, L. Faure, M. C. Lagomarsino, and S. van Teeffelen, Elife **10**, e67495 (2021).
[15] F. D. C. Farrell, O. Hallatschek, D. Marenduzzo, and B. Waclaw, Phys. Rev. Lett. **111**, 168101 (2013).
[16] F. D. Farrell, M. Gralka, O. Hallatschek, and B. Waclaw, J. R. Soc. Interface **14**, 20170073 (2017).
[17] S. K. Schnyder, J. J. Molina, and R. Yamamoto, Sci. Rep. **10**, 6713 (2020).
[18] B. Langeslay and G. Juarez, arXiv preprint arXiv:2212.00233 (2022).
[19] J. Dhar, A. L. P. Thai, A. Ghoshal, L. Giomi, and A. Sengupta, Nat. Phys. **18**, 945 (2022).
[20] A. Puliafito, L. Hufnagel, P. Neveu, S. Streichan, A. Sigal, D. K. Fygenson, and B. I. Shraiman, Proc. Natl. Acad. Sci. U.S.A. **109**, 739 (2012).
[21] U. M. B. Marconi and P. Tarazona, J. Chem. Phys. **110**, 8032 (1999).
[22] A. J. Archer and R. Evans, J. Chem. Phys. **121**, 4246 (2004).
[23] M. te Vrugt, H. Löwen, and R. Wittkowski, Adv. Phys. **69**, 121 (2020).

[24] A. Chauviere, H. Hatzikirou, I. G. Kevrekidis, J. S. Lowengrub, and V. Cristini, AIP Adv. **2**, 011210 (2012).
[25] H. M. Al-Saedi, A. J. Archer, and J. Ward, Phys. Rev. E **98**, 022407 (2018).
[26] See Supplemental Material at [URL will be inserted by publisher] for an introduction of the general DDFT including position- and orientation dependence, analytic solutions of the length-resolved DDFT, simulation description and experimental details.
[27] C. D. Cox, N. Bavi, and B. Martinac, Annu. Rev. Physiol **80**, 71 (2018).
[28] V. D. Gordon and L. Wang, J. Cell Sci. **132**, jcs227694 (2019).
[29] Nicola Pellicciotta, private communication.
[30] A. J. Archer and R. Evans, Phys. Rev. E **64**, 041501 (2001).
[31] R. Evans, Adv. Phys. **28**, 143 (1979).
[32] T. K. Vanderlick, H. T. Davis, and J. K. Percus, J. Chem. Phys. **91**, 7136 (1989).
[33] R. Wittmann, C. E. Sitta, F. Smallenburg, and H. Löwen, J. Chem. Phys. **147**, 134908 (2017).
[34] R. Wittmann, M. Marechal, and K. Mecke, J. Phys. Condens. Matter **28**, 244003 (2016).
[35] K. S. Korolev, M. Avlund, O. Hallatschek, and D. R. Nelson, Rev. Mod. Phys. **82**, 1691 (2010).
[36] S. Pigolotti, R. Benzi, M. H. Jensen, and D. R. Nelson, Phys. Rev. Lett. **108**, 128102 (2012).
[37] F. Beroz, J. Yan, Y. Meir, B. Sabass, H. A. Stone, B. L. Bassler, and N. S. Wingreen, Nat. Phys. **14**, 954 (2018).
[38] A. Amir, Phys. Rev. Lett. **112**, 208102 (2014).
[39] A. Delgado-Campos and A. Cuetos, Phys. Rev. E **106**, 034402 (2022).
[40] N. Allocati, M. Masulli, C. Di Ilio, and V. De Laurenzi, Cell Death Dis. **6**, e1609 (2015).
[41] P. Ghosh and H. Levine, Phys. Rev. E **96**, 052404 (2017).
[42] H. T. K. Tse, W. M. Weaver, and D. Di Carlo, PloS one **7**, e38986 (2012).
[43] I. Frost, W. P. J. Smith, S. Mitri, A. S. Millan, Y. Davit, J. M. Osborne, J. M. Pitt-Francis, R. C. MacLean, and K. R. Foster, ISME J. **12**, 1582 (2018).
[44] J. Li, S. K. Schnyder, M. S. Turner, and R. Yamamoto, Phys. Rev. Res. **4**, 033156 (2022).
[45] N. Q. Balaban, J. Merrin, R. Chait, L. Kowalik, and S. Leibler, Science **305**, 1622 (2004).
[46] E. Kussell and S. Leibler, Science **309**, 2075 (2005).
[47] M. Wrande, J. R. Roth, and D. Hughes, Proc. Natl. Acad. Sci. U.S.A. **105**, 11863 (2008).

[48] R. Hashuel and S. Ben-Yehuda, MBio **10**, e01414 (2019).

[49] L. Mederos, E. Velasco, and Y. Martínez-Ratón, J. Phys. Condens. Matter **26**, 463101 (2014).

[50] H.-P. Zhang, A. Be'er, E.-L. Florin, and H. L. Swinney, Proc. Natl. Acad. Sci. U.S.A. **107**, 13626 (2010).

[51] J. Liu, A. Prindle, J. Humphries, M. Gabalda-Sagarra, M. Asally, D.-Y. D. Lee, S. Ly, J. Garcia-Ojalvo, and G. M. Süel, Nature **523**, 550 (2015).

[52] P. Bera, A. Wasim, and P. Ghosh, bioRxiv (2022).

[53] W. Pönisch, K. B. Eckenrode, K. Alzurqa, H. Nasrollahi, C. Weber, V. Zaburdaev, and N. Biais, Sci. Rep. **8**, 16567 (2018).

[54] H.-S. Kuan, W. Pönisch, F. Jülicher, and V. Zaburdaev, Phys. Rev. Lett. **126**, 018102 (2021).

[55] M. Basaran, Y. I. Yaman, T. C. Yüce, R. Vetter, and A. Kocabas, Elife **11**, e72187 (2022).

[56] D. Volfson, S. Cookson, J. Hasty, and L. S. Tsimring, Proc. Natl. Acad. Sci. U.S.A. **105**, 15346 (2008).

[57] N. Podewitz, M. Delarue, and J. Elgeti, Europhys. Lett. **109**, 58005 (2015).

[58] Z. You, D. J. G. Pearce, and L. Giomi, Sci. Adv. **7**, eabc8685 (2021).

[59] T. Shimaya and K. A. Takeuchi, arXiv preprint arXiv:2106.10954 (2021).

[60] A. Doostmohammadi, S. P. Thampi, and J. M. Yeomans, Phys. Rev. Lett. **117**, 048102 (2016).

[61] D. Dell'Arciprete, M. L. Blow, A. T. Brown, F. D. C. Farrell, J. S. Lintuvuori, A. F. McVey, D. Marenduzzo, and W. C. K. Poon, Nat. Commun. **9**, 4190 (2018).

[62] D. v. H. t. Echten, G. Nordemann, M. Wehrens, S. Tans, and T. Idema, arXiv preprint arXiv:2003.10509 (2020).

[63] A. Sengupta, Front. Phys. **8**, 184 (2020).

[64] D. Boyer, W. Mather, O. Mondragón-Palomino, S. Orozco-Fuentes, T. Danino, J. Hasty, and L. S. Tsimring, Phys. Biol. **8**, 026008 (2011).

[65] R. Wittmann, L. B. G. Cortes, H. Löwen, and D. G. A. L. Aarts, Nat. Commun. **12**, 1 (2021).

[66] P. A. Monderkamp, R. Wittmann, L. B. G. Cortes, D. G. A. L. Aarts, F. Smallenburg, and H. Löwen, Phys. Rev. Lett. **127**, 198001 (2021).

[67] J. Xia, S. MacLachlan, T. J. Atherton, and P. E. Farrell, Phys. Rev. Lett. **126**, 177801 (2021).

[68] J. Paget, M. G. Mazza, A. J. Archer, and T. N. Shendruk, arXiv preprint arXiv:2201.09019 (2022).

[69] K. Drescher, J. Dunkel, C. D. Nadell, S. Van Teeffelen, I. Grnja, N. S. Wingreen, H. A. Stone, and B. L. Bassler, Proc. Natl. Acad. Sci. U.S.A. **113**, E2066 (2016).

[70] M. R. Warren, H. Sun, Y. Yan, J. Cremer, B. Li, and T. Hwa, Elife **8**, e41093 (2019).

[71] B. Ni, R. Colin, H. Link, R. G. Endres, and V. Sourjik, Proc. Natl. Acad. Sci. U.S.A. **117**, 595 (2020).

[72] D. Breoni, F. J. Schwarzendahl, R. Blossey, and H. Löwen, Eur. Phys. J. E **45**, 83 (2022).

[73] D. B. Ingham and I. Pop, *Transport phenomena in porous media* (Elsevier, 1998).

[74] D. Or, B. F. Smets, J. M. Wraith, A. Dechesne, and S. P. Friedman, Adv. Water Resour. **30**, 1505 (2007).

[75] P. Ghosh, J. Mondal, E. Ben-Jacob, and H. Levine, Proc. Natl. Acad. Sci. U.S.A. **112**, E2166 (2015).

[76] R. Hornung, A. Grünberger, C. Westerwalbesloh, D. Kohlheyer, G. Gompper, and J. Elgeti, J. R. Soc. Interface **15**, 20170713 (2018).

[77] O. Fridman, A. Goldberg, I. Ronin, N. Shoresh, and N. Q. Balaban, Nature **513**, 418 (2014).

[78] K. M. Kauffman, W. K. Chang, J. M. Brown, F. A. Hussain, J. Yang, M. F. Polz, and L. Kelly, Nat. Commun. **13**, 1 (2022).

[79] K. R. Elder, N. Provatas, J. Berry, P. Stefanovic, and M. Grant, Phys. Rev. B **75**, 064107 (2007).

[80] S. van Teeffelen, R. Backofen, A. Voigt, and H. Löwen, Phys. Rev. E **79**, 051404 (2009).

[81] K. R. Elder, M. Katakowski, M. Haataja, and M. Grant, Phys. Rev. Lett. **88**, 245701 (2002).

[82] A. Doostmohammadi, J. Ignés-Mullol, J. M. Yeomans, and F. Sagués, Nat. Commun. **9**, 3246 (2018).

[83] S. Berg, D. Kutra, T. Kroeger, C. N. Straehle, B. X. Kausler, C. Haubold, M. Schiegg, J. Ales, T. Beier, M. Rudy, et al., Nat. Methods **16**, 1226 (2019).

Supplementary Material: Mechano-self-regulation of bacterial size in growing colonies

I. GENERAL THEORY FOR BACTERIAL GROWTH

In this supplemental section we derive our main equation, Eq. (3), of the main text and provide the theoretical background on dynamical density functional theory (DDFT). Section I A introduces our general position- and orientation-resolved DDFT model for growing colonies, which includes the dynamics of the particle length. Section I B then discusses the coarse-grained version of our DDFT model analyzed in the main text to describe the phenotemporal dynamics only. Section I C shows how a bare growth equation for the average density can be obtained upon further coarse graining.

A. DDFT for growing bacterial colonies

To derive our general DDFT model for growing bacterial colonies, we proceed in three steps. First, in Sec. I A 1, we briefly introduce the basic concept of DDFT by considering a polydisperse mixtures of orientable particles of length l. Second, in Sec. I A 2, we demonstrate how to use DDFT for growing bacteria whose length changes over time by identifying additional terms that describe fluctuations and interactions affecting the dependence on l itself and adding a growth term to drive the system out of equilibrium. Finally, in Sec. I A 3, we discuss how to incorporate cell division.

1. DDFT for polydisperse particle lengths

To describe a polydisperse mixture of particles with different length l (or, more generally, different sizes), we consider the time-dependent one-body number density $\rho(\mathbf{r}, \mathbf{p}, l, t)$, which has dimension of inverse volume times inverse particle length. In such a system, each particle has a fixed length l, such that the total number $N = \int d\mathbf{r} \int d\mathbf{p} \int dl\, \rho(\mathbf{r}, \mathbf{p}, l, t)$ of particles and also the length distribution $h(l) = \int d\mathbf{r} \int d\mathbf{p}\, \rho(\mathbf{r}, \mathbf{p}, l, t)/N$ remain independent of time.

The idea of dynamical density functional theory (DDFT) [21–23] is that, at a time t, the instantaneous time-dependent density $\rho(\mathbf{r}, \mathbf{p}, l, t)$ gives rise to nonequilibrium currents, generated from an equilibrium free energy, which themselves drive the time evolution of the density according to the continuity equation

$$\frac{\partial \rho(\mathbf{r}, \mathbf{p}, l, t)}{\partial t} = -\boldsymbol{\nabla}_{\mathbf{r}} \cdot \mathbf{J}_{\mathbf{r}}(\mathbf{r}, \mathbf{p}, l, t) - \hat{\mathcal{R}}_{\mathbf{p}} \cdot \mathbf{J}_{\mathbf{p}}(\mathbf{r}, \mathbf{p}, l, t)\,, \tag{7}$$

where $\boldsymbol{\nabla}_{\mathbf{r}}$ is the spatial gradient, $\hat{\mathcal{R}}_{\mathbf{p}} = \mathbf{p} \times \boldsymbol{\nabla}_{\mathbf{p}}$ is the rotation operator and $\beta = (k_{\mathrm{B}}T)^{-1}$ denotes the inverse temperature with Boltzmann's constant k_{B} to provide the energy scale. The currents have the general form

$$\mathbf{J}_{\mathbf{r}}(\mathbf{r}, \mathbf{p}, l, t) = -D_{\mathbf{r}} \boldsymbol{\nabla}_{\mathbf{r}} \rho(\mathbf{r}, \mathbf{p}, l, t) - D_{\mathbf{r}} \rho(\mathbf{r}, \mathbf{p}, l, t) \boldsymbol{\nabla}_{\mathbf{r}} \frac{\delta \beta \mathcal{F}_{\mathrm{ex}}[\rho]}{\delta \rho(\mathbf{r}, \mathbf{p}, l, t)} - D_{\mathbf{r}} \rho(\mathbf{r}, \mathbf{p}, l, t) \boldsymbol{\nabla}_{\mathbf{r}} \beta V_{\mathrm{ext}}(\mathbf{r}, \mathbf{p}, l)\,,$$

$$\mathbf{J}_{\mathbf{p}}(\mathbf{r}, \mathbf{p}, l, t) = -D_{\mathbf{p}} \hat{\mathcal{R}}_{\mathbf{p}} \rho(\mathbf{r}, \mathbf{p}, l, t) - D_{\mathbf{p}} \rho(\mathbf{r}, \mathbf{p}, l, t) \hat{\mathcal{R}}_{\mathbf{p}} \frac{\delta \beta \mathcal{F}_{\mathrm{ex}}[\rho]}{\delta \rho(\mathbf{r}, \mathbf{p}, l, t)} - D_{\mathbf{p}} \rho(\mathbf{r}, \mathbf{p}, l, t) \hat{\mathcal{R}}_{\mathbf{p}} \beta V_{\mathrm{ext}}(\mathbf{r}, \mathbf{p}, l)\,, \tag{8}$$

where $D_{\mathbf{r}}$ and $D_{\mathbf{p}}$ denote the translational and rotational diffusion coefficients, respectively. In both cases, the first term describes ideal diffusion, while the second and third terms describe a drift due to interactions. In the spirit of equilibrium density functional theory (DFT) [31], the (pairwise) interactions between the particles can be conveniently expressed by an excess free energy functional $\mathcal{F}_{\mathrm{ex}}$, whose functional derivative is used to construct an approximate expression for the average interaction force in DDFT. Moreover, the external potential $V_{\mathrm{ext}}(\mathbf{r}, \mathbf{p}, l)$ models the interaction of each particle with an externally imposed field.

The standard form (7) of DDFT describes the time evolution of a polydisperse fluid in its approach to thermodynamic equilibrium. To describe a nonequilibrium system of growing bacteria it is vital to give up the notion that the length l is a fixed particle property, as we will do next.

2. Growth, fluctuations and interactions

Our general model for growing bacterial colonies involves the additional current

$$J_l(\mathbf{r}, \mathbf{p}, l, t) = -D_l \frac{\partial \rho(\mathbf{r}, \mathbf{p}, l, t)}{\partial l} - \tilde{D}_l \left(\rho(\mathbf{r}, \mathbf{p}, l, t) \left(\frac{\partial}{\partial l} \frac{\delta \beta \mathcal{F}_{\text{ex}}[\rho]}{\delta \rho(\mathbf{r}, \mathbf{p}, l, t)} + \frac{\partial \beta V_{\text{ext}}(\mathbf{r}, \mathbf{p}, l)}{\partial l} \right) \right) + G \rho(\mathbf{r}, \mathbf{p}, l, t) \qquad (9)$$

which describes how the length-dependent part of the density changes over time. In contrast to the typical form (8) of a current which describes the approach of equilibrium, our length current J_l has two ingredients which are of nonequilibrium nature. First, there is an additional last term on the right-hand side of Eq. (9) that is not derived from the free energy $\mathcal{F}[\rho]$. It describes a drift in the length variable l with velocity $G \geq 0$, which models the bacterial growth and drives the system out of equilibrium. Second, in nonequilibrium, there is no fixed relation between the prefactor of the first diffusive and second interaction terms, such that it makes sense to introduce different diffusion-type coefficients D_l and $\tilde{D}_l$, respectively, to characterize the distinct physical effects modeled by these terms. Specifically, the first term on the right-hand side of Eq. (9) describes a fluctuation of the bacterial lengths which results in the tendency to smoothen out the distribution. Thus it models that the (average) elongation rate G actually fluctuates as a function of time, while the variance of these fluctuations is measured by the parameter D_l. The second term on the right-hand side of Eq. (9) describes the steric forces acting on the growing particles due to the presence of other particles (internal interactions are represented by the excess free energy $\mathcal{F}_{\text{ex}}[\rho]$) or possible system boundaries (external interactions are represented by the external potential V_{ext}). These mechanical interactions also describe a drift in the length variable l and thus regulate the bacterial growth, i.e., the parameter $\tilde{D}_l$ models the strength of mechano-self-regulation, which seeks to shrink the particles in order to increase the free volume per particle, thereby counteracting the growth process. While this effect is not included in most models for growing bacteria, it constitutes a natural and physically sensible extension: the colony only grows up to a certain average density, at which the steric interactions and the drift of lengths are in balance, thus eventually reaching a nonequilibrium steady state.

In conclusion, the length current (9) is introduced to model the bacterial growth which is subject to fluctuations and self regulation. Together with positional and orientational currents from Eq. (8), the generalization of Eq. (7) yields the DDFT equation

$$\frac{\partial \rho(\mathbf{r}, \mathbf{p}, l, t)}{\partial t} = -\boldsymbol{\nabla}_{\mathbf{r}} \cdot \mathbf{J}_{\mathbf{r}}(\mathbf{r}, \mathbf{p}, l, t) - \hat{\mathcal{R}}_{\mathbf{p}} \cdot \mathbf{J}_{\mathbf{p}}(\mathbf{r}, \mathbf{p}, l, t) - \frac{\partial}{\partial l} J_l(\mathbf{r}, \mathbf{p}, l, t) \qquad (10)$$

for bacterial growth. Note that the spatial forces, orientational torques and mechano-self-regulation of bacterial growth have the same physical origin, as they are all follow from the same model interactions. What is left to be specified below is the domain of the length variable l.

3. Cell division

To include cell division in our model, we assume that each bacterium grows until its length l has reached the value $2L$ and then divide into two daughter cells of half length L, which is called the length-at-birth. To incorporate this effect in Eq. (10), we introduce as our basic model additional source and sink terms determined by the length current for $l = 2L$ and assume that l is restricted to the interval $[L, 2L]$ with a periodic boundary condition. Then, our general DDFT becomes

$$\frac{\partial \rho(\mathbf{r}, \mathbf{p}, l, t)}{\partial t} = -\boldsymbol{\nabla}_{\mathbf{r}} \cdot \mathbf{J}_{\mathbf{r}}(\mathbf{r}, \mathbf{p}, l, t) - \hat{\mathcal{R}}_{\mathbf{p}} \cdot \mathbf{J}_{\mathbf{p}}(\mathbf{r}, \mathbf{p}, l, t) - \frac{\partial}{\partial l} J_l(\mathbf{r}, \mathbf{p}, l, t)$$
$$+ \delta(l - L) J_l \left(\mathbf{r} + \frac{L}{2} \mathbf{p}, \mathbf{p}, 2L, t \right) + \delta(l - L) J_l \left(\mathbf{r} - \frac{L}{2} \mathbf{p}, \mathbf{p}, 2L, t \right) - \delta(l - 2L) J_l(\mathbf{r}, \mathbf{p}, 2L, t) , \quad (11)$$

i.e., the bacteria with $l = 2L$ are removed, while two new bacteria with $l = L$ are inserted at shifted centers. Note that this way of implementing cell division does not necessarily require us to restrict the particle length to the interval $l \in [L, 2L]$ and, in fact, it will turn out to be important to specify in more detail what exactly happens at the boundary in l for later times. This will be investigated in more detail in Sec. II C 2, where we also discuss an alternative boundary condition and a refined implementation of cell division compared to our basic model, Eq. (11).

B. Coarse-grained phenotemporal DDFT for a spatially homogeneous and isotropic system

In the main manuscript, we are only interested in the coarse-grained phenotemporal dynamics of the density $\rho(l,t) = \int d\mathbf{r} \int d\mathbf{p}\, \rho(\mathbf{r}, \mathbf{p}, l)/V$ only resolving the length l (or generally the phenotype) of the bacteria and not their spatial position $\mathbf{r}$ or orientation $\mathbf{p}$. Thus, we introduce in Sec. I B 1 that the coarse-grained version of Eq. (11) before deriving in Sec. I B 2 the DDFT equation discussed in the main manuscript.

1. Different versions of the general theory

In a spatially homogeneous system all spatial and orientational derivatives vanish. The dynamics of $\rho(l,t)$ are described by the coarse-grained DDFT equation

$$\frac{\partial \rho(l,t)}{\partial t} = -\frac{\partial}{\partial l} J_l(l,t) + 2\delta(l-L)J_l(2L,t) - \delta(l-2L)J_l(2L,t) \tag{12}$$

with $l \in [L, 2L]$ and the current

$$J_l(l,t) = -D_l \frac{\partial \rho(l,t)}{\partial l} - \tilde{D}_l \rho(l,t)\frac{\partial}{\partial l}\frac{\delta \beta \mathcal{F}_{\text{ex}}[\rho]}{V \delta \rho(l,t)} - \tilde{D}_l \rho(l,t)\frac{\partial}{\partial l}\beta V_{\text{ext}}(l) + G\,\rho(l,t)\,. \tag{13}$$

Note that, compared to the current in Eq. (9), the external potential $V_{\text{ext}}(l)$ should only act on the bacterial length and the factor $1/V$ in front of the functional derivative compensates the missing argument $\mathbf{r}$ of the density with respect to which the functional derivative is taken. This is our general DDFT model for the length distribution of growing bacterial colonies.

Without positional dependence, cell division merely amounts to doubling the number of particles. Thus it can be modeled in an alternative and more convenient way by simply considering an explicit boundary condition on the periodic interval $l \in [L, 2L]$. Specifically, we recast Eq. (12) as

$$\frac{\partial \rho(l,t)}{\partial t} = -\frac{\partial}{\partial l} J_l(l,t) \tag{14}$$

with the oblique boundary condition

$$\rho(L,t) = 2\rho(2L,t)\,, \tag{15}$$

at any time t. Due to the absence of source terms, the explicit solution of Eq. (14) is strongly facilitated. Further details on the role of boundary conditions will be discussed in Sec. II C 2.

2. Explicit DDFT equation for mean-field interactions

Now, let us consider the specific model for a freely growing colony in the absence of an external potential $V_{\text{ext}}(l,t) \equiv 0$ and a mean-field type repulsive interaction. We thus choose the excess free energy

$$\mathcal{F}_{\text{ex}}[\rho] = \frac{1}{2}\int dl \int dl'\, \rho(l,t)u(l,l')\rho(l',t) \tag{16}$$

with the coarse-grained pair potential

$$\beta u(l,l') = \int d\mathbf{r} \int d\mathbf{r}'\, \beta U(\mathbf{r}, \mathbf{r}, l, l') = \tilde{S}(l+l')V\,, \tag{17}$$

which corresponds to the double spatial integral of a Gaussian pair potential $U(\mathbf{r}, \mathbf{r}, l, l')$ of width $l + l'$. The positive parameter $\tilde{S}$ represents the integrated repulsion strength and has the dimension of volume over particle length. A suitable alternative choice for $\mathcal{F}_{\text{ex}}$ would be fundamental measure theory (FMT), modeling the bacteria as mixtures of hard rods in one [32] two [33] or three [34] spatial dimensions.

Before proceeding, let us define a normalized length distribution $h(l,t)$ such that

$$\int dl\, h(l,t) = 1 \tag{18}$$

and the average density

$$\bar{\rho}(t) = \int \mathrm{d}l\, \rho(l, t) \tag{19}$$

such that we can conveniently write the density as

$$\rho(l, t) = \bar{\rho}(t)\, h(l, t)\,. \tag{20}$$

Inserting now Eq. (16) into Eq. (13) yields the current

$$J_l = -D\partial_l \rho(l, t) - S\rho(l, t)\bar{\rho}(t) + G\rho(l, t) \tag{21}$$

where we have redefined $D = D_l$ and $S = \tilde{D}_l \tilde{S}$ to arrive at the notation of the main manuscript. This finally yields the DDFT model

$$\frac{\partial \rho(l, t)}{\partial t} = \bar{\rho}(t)\frac{\partial}{\partial l}\left(D\frac{\partial}{\partial l}h(l, t) + Sh(l, t)\bar{\rho}(t) - Gh(l, t)\right)\,. \tag{22}$$

stated as Eq. (2) of the main manuscript, together with the boundary condition on the periodic interval $l \in [L, 2L]$ given by Eq. (15).

C. Coarse-grained growth equation

Finally, we demonstrate how to coarse grain Eq. (22) if one is only interested in the growth of the average density. As we will see later, it is a sensible approximation to assume that the length distribution

$$h(l, t) = \frac{4\ln 2}{L}2^{-l/L} \tag{23}$$

is uniform and independent of time. With this assumption we can evaluate all derivatives with respect to l and then eliminate $h(l, t)$ from the equation to obtain the coarse-grained dynamics of the average density $\bar{\rho}(t)$. As stated in the main manuscript, this growth equation reads

$$\frac{\partial \bar{\rho}(t)}{\partial t} = \bar{\rho}(t)(R - S_\mathrm{u}\bar{\rho}(t)) \tag{24}$$

with the parameters

$$R = \left(G + D\frac{\ln 2}{L}\right)\frac{\ln(2)}{L}\,, \quad S_\mathrm{u} = S\frac{\ln(2)}{L}\,. \tag{25}$$

Alternatively we could have integrated both sides of Eq. (22) over l and used the boundary condition from Eq. (15) explicitly. It can be shown that the solution of Eq. (24) is

$$\bar{\rho}(t) = \frac{R\bar{\rho}_0}{S_\mathrm{u}\bar{\rho}_0 + (R - S_\mathrm{u}\bar{\rho}_0)e^{-Rt}}\,, \tag{26}$$

where $\bar{\rho}_0 := \bar{\rho}(0)$ is the initial average number density, as stated in Eq. (4) of the main manuscript.

II. EVALUATION OF THE PHENOTEMPORAL DDFT FOR BACTERIAL GROWTH

In this supplemental section we discuss the solution of our DDFT for growing bacterial colonies, Eq. (22). After discussing in Sec. II A the dimensions of the different ingredients, we elaborate on the analytic progress that can be made in Sec. II B Then we provide details on the numerics and present additional results in Sec. II C.

A. Nondimensional units

Before proceeding with the solution of Eq. (22), we take a closer look at its ingredients. As already discussed in Sec. I A, the density $\rho(l,t) = \bar{\rho}(t)\,h(l,t)$ has the units of inverse volume times inverse length, while the former is included in the average density $\bar{\rho}(t)$ and the latter in the length distribution $h(l,t)$. Assuming that at the initial time $t = 0$ the colony starts to grow from a single bacterium, then the initial average number density is given by $\bar{\rho}_0 := \bar{\rho}(0) = 1/V$ where V is the system volume. For the sake of generality, we conveniently take $\bar{\rho}_0^{-1}$ as our unit volume and the bacterial length L as unit length.

From the three free parameters in Eq. (22), we can identify the three time scales

$$\frac{L^2}{D}\,, \quad \frac{L}{S\bar{\rho}_0}\,, \quad \frac{L}{G}\,. \tag{27}$$

Choosing L/G as our time unit, we find the equation

$$\frac{\partial N(\tilde{l},\tilde{t})}{\partial \tilde{t}} = n(\tilde{t})\frac{\partial}{\partial \tilde{l}}\left(d\frac{\partial}{\partial \tilde{l}}\tilde{h}(\tilde{l},\tilde{t}) + s\tilde{h}(\tilde{l},\tilde{t})\,n(\tilde{t}) - \tilde{h}(\tilde{l},\tilde{t})\right) \tag{28}$$

with the dimensionless quantities

$$\tilde{t} = t\frac{G}{L}\,, \quad \tilde{l} = \frac{l}{L}\,, \quad d = \frac{D}{GL}\,, \quad s = \frac{S\bar{\rho}_0}{G}\,, \quad N(\tilde{l},\tilde{t}) = \rho(l,t)\frac{L}{\bar{\rho}_0}\,, \quad n(\tilde{t}) = \bar{\rho}(t)\frac{1}{\bar{\rho}_0}\,, \quad \tilde{h}(\tilde{l},\tilde{t}) = h(l,t)L\,. \tag{29}$$

B. Analytic insight

Now we derive and analyze the analytic results behind the length distributions shown in Fig. 2 of the main manuscript. To this end we discuss the full or stationary solution of Eq. (22), with the oblique boundary condition given by Eq. (15), for some special choices of parameters.

1. Oscillating growth

Let us first consider the bare growth process with $D = S = 0$ and $G > 0$, which is described by the linear first-order partial differential equation

$$\frac{\partial \rho(l,t)}{\partial t} = -G\frac{\partial \rho(l,t)}{\partial l}\,. \tag{30}$$

A drift equation of this form is in general solved by any function $F(l - tG)$, where $t \geq 0$ and $l \in \mathbb{R}$. Together with the initial condition $h_0(l) := h(l,0)$ for the length distribution we can formally determine the effective particular solution

$$\varrho(l,t) = \bar{\rho}_0\,h_0(l - tG) \tag{31}$$

for a more general length variable l defined on an infinite domain, i.e., $l/L \in \mathbb{R}$, recalling that $h_0(l) = 0$ if $l < L$ or $l > 2L$. Since in our case we always require a solution $\rho(l,t)$ with $l \in [L, 2L]$ on a restricted interval, our boundary condition (15) must be explicitly built into the final solution deduced from this $\varrho(l,t)$.

To do so for this particular example, we keep in mind the physical meaning of the underlying drift equation (30). Assuming that a bacterium without cell division continues to grow for the time nL/G, where n is a positive integer number, its length $l \in \mathbb{R}$ has increased by nL. For $l \in [L, 2L]$, the same consideration tells us that a bacterium has undergone n division events after time nL/G. Likewise, after a general time t, a bacterium with length l has divided for

$$n := 1 - \left\lfloor \frac{l - Gt}{L} \right\rfloor = \left\lceil \frac{Gt - l + L}{L} \right\rceil \tag{32}$$

times, where the Gaussian brackets evaluate the included expression to the closest smaller or larger integer, respectively. Now we can include our boundary condition, which doubles the density at a division event, to construct our desired result

$$\rho(l,t) = \bar{\rho}_0 \, 2^n \, h_0(l - Gt + nL) \tag{33}$$

from the effective solution $\varrho(l,t)$ in Eq. (31), while the time- and length-dependent division number n is given by Eq. (32). For a general effective density $\varrho(l,t)$ with $l/L \in \mathbb{R}$ the argumentation outlined above results in

$$\rho(l,t) = \sum_{n=-\infty}^{\infty} 2^n \varrho(l + nL, t), \tag{34}$$

where, at time t, only those terms need to be considered which give a significant contribution for the domain $l \in [L, 2L]$ of $\rho(l,t)$. In the present example, the two terms with n given by Eq. (32) are sufficient.

Having obtained $\rho(l,t)$ at given time t, the integration over l allows us to identify the growth of the average number density $\bar{\rho}(t)$. From the explicit formula in Eq. (33) we find

$$\bar{\rho}(t) = \bar{\rho}_0 \, 2^m \left(\int_L^{2L+Gt-mL} \mathrm{d}l \, h_0(l - Gt + mL) + \frac{1}{2} \int_{2L+Gt-mL}^{2L} \mathrm{d}l \, h_0(l - Gt + (m-1)L) \right)$$

$$= \bar{\rho}_0 \, 2^m \left(\int_{(m+1)L-tG}^{2L} \mathrm{d}l' \, h_0(l') + \frac{1}{2} \int_L^{(m+1)L-tG} \mathrm{d}l' \, h_0(l') \right) \quad \text{with} \quad m := \left\lceil \frac{Gt}{L} \right\rceil . \tag{35}$$

Therefore, the normalized length distribution $h(l,t) = \frac{\rho(l,t)}{\bar{\rho}(t)}$ is a periodic function of time with period L/G, as shown in Fig. 2A of the main manuscript. This result motivates the choice of L/G as our unit time scale.

The exponential initial condition $h_0(l) = \frac{4\ln 2}{L} 2^{-l/L}$ gives rise to a special case since then $h(l,t)$ remains in exactly the same form for all times, as assumed in Eq. (23). Then the formula in Eq. (35) reduces to $\bar{\rho}(t) = \bar{\rho}_0 \, 2^{Gt/L}$, which corresponds to the expression (26) with $R = G \ln 2/L$ and $S_\mathrm{u} = 0$ obtained from the coarse-grained growth equation.

2. Retarded growth

Next, we also allow for mechanical forces, considering $G, S > 0$ and $D = 0$ in Eq. (22), such that the elongation rate is effectively reduced when the density increases. This scenario is described by the nonlinear first-order partial differential equation

$$\frac{\partial \rho(l,t)}{\partial t} = -(G - S\bar{\rho}(t)) \frac{\partial \rho(l,t)}{\partial l} =: -G_{\mathrm{eff},0}(t) \frac{\partial \rho(l,t)}{\partial l} , \tag{36}$$

where we have identified $G_{\mathrm{eff},0}(t)$ as an effective elongation rate due to mechano-self-regulation. Since the length-dependent part of this equation is the same as in Eq. (30), the form of $h(l,t)$ is related to the given initial distribution $h_0(l)$ in a similar way as elaborated for $S = 0$ in Sec. II B 1. However, the length Δt of the time intervals where $h(l, t + \Delta t) = h(l,t)$ returns to its earlier form increases with time, since the effective drift velocity decreases due to steric repulsion, as shown in Fig. 2B of the main manuscript. The particular dynamics of $\rho(l,t)$ are implicitly given by substituting $G \to G - S\bar{\rho}(t)$ in Eqs. (33) and (32).

As before, for $h_0(l) = \frac{4\ln 2}{L} 2^{-l/L}$ the time evolution of $h(l,t)$ remains uniform and $\bar{\rho}(t)$ is given by Eq. (26) with $R = G \ln 2/L$ and $S_\mathrm{u} = S \ln 2/L$. This result can be used to provide an approximate solution for the full $\rho(l,t)$ with an arbitrary initial length distribution $h_0(l)$. Solving Eq. (36) under the assumption that $G_{\mathrm{eff},0}(t)$ does not explicitly depend on the density, we can approximately generalize Eq. (31) to

$$\varrho(l,t) \approx \bar{\rho}_0 \, h_0 \left(l - \int_0^t G_{\mathrm{eff},0}(t') \mathrm{d}t' \right) \tag{37}$$

and then insert the analytic $\bar{\rho}(t)$ from Eq. (26) into $G_{\mathrm{eff},0}(t) = G - S\bar{\rho}(t)$. This result can then be inserted in Eq. (34) to obtain $\rho(l,t)$ and then also a better approximation for $\bar{\rho}(t)$ and $G_{\mathrm{eff},0}(t)$. Equations (33) and (32) can be generalized accordingly.

3. Uniform growth

Next we consider the situation with fluctuating growth but in the absence of mechano-self-regulation, setting $D, G > 0$ and $S = 0$ in Eq. (22), which becomes

$$\frac{\partial \rho(l,t)}{\partial t} = D\frac{\partial^2 \rho(l,t)}{\partial l^2} - G\frac{\partial \rho(l,t)}{\partial l} \; . \tag{38}$$

Without mechanical force, the growth of the colony is again unlimited, such that no stationary state is reached. However, the fluctuations change the length distribution, such that its shape becomes as uniform as compatible with the boundary condition (15), as shown in Fig. 2C of the main manuscript. Starting with a sharp length distribution at time $t = 0$, representing a single bacterium with initial length $l_0 \in [L, 2L]$, we may choose the initial condition $\varrho(l,0) = \rho(l,0) = \bar{\rho}_0\delta(l - l_0)$ given by the Dirac-delta distribution or, more generally, by a Gaussian distribution of width w_0. Then the drift-diffusion equation (22) has the effective particular solution

$$\varrho(l,t) = \bar{\rho}_0 \frac{\exp\left(-\frac{(l-l_0-Gt)^2}{2(\sigma_0^2+2Dt)}\right)}{\sqrt{2\pi}(\sigma_0 + \sqrt{2Dt})} \tag{39}$$

on the infinite domain $l/L \in \mathbb{R}$, from which we can formally construct the solution $\rho(l,t)$ appropriate for $l \in [L, 2L]$ according to Eq. (34).

We can make more explicit analytical progress upon assuming that there exists a stationary length distribution $h_\infty(l)$ after a certain time t_0, we can write the time-dependent density as $\rho(l,t) = \bar{\rho}(t)h_\infty(l)$. Plugging this ansatz into Eq. (38), it reduces to the evolution equation

$$\frac{\partial \bar{\rho}(t)}{\partial t} = \bar{\rho}(t)\frac{1}{h_\infty(l)}\frac{\partial}{\partial l}\left(D\frac{\partial h_\infty(l)}{\partial l} - Gh_\infty(l)\right) =: R\bar{\rho}(t) \tag{40}$$

for $\bar{\rho}(t)$, where the constant R must not depend on the length l by definition of $\bar{\rho}(t)$. Defining $\bar{\rho}_0 := \bar{\rho}(t_0)$ this equation can be solved as

$$\bar{\rho}(t) = \bar{\rho}_0\,e^{Rt} \; , \tag{41}$$

where the condition

$$Rh_\infty(l) = \frac{\partial}{\partial l}\left(D\frac{\partial h_\infty(l)}{\partial l} - Gh_\infty(l)\right) \tag{42}$$

with parameter R that must be independent of l has the solution

$$h_\infty(l) = \frac{4\ln 2}{L}\,2^{-\frac{l}{L}} \; , \tag{43}$$

$$R = \ln 2\left(\ln 2\frac{D}{L^2} + \frac{G}{L}\right) \; . \tag{44}$$

Thus there exists a unique stationary length distribution which has an exponential shape as assumed in Eq. (23). Indeed, the parameter R is exactly the same as that, given by Eq. (25), in out coarse-grained growth equation and through Eq. (41) we have recovered Eq. (26) with $S_\mathrm{u} = 0$.

4. Retarded uniform growth

Combining the efforts of the previous section, we can obtain the approximate solution of Eq. (22) with all parameters $D, S, G > 0$ nonvanishing from the effective density

$$\varrho(l,t) = \bar{\rho}_0 \frac{\exp\left(-\frac{\left(l-l_0-\int_0^t G_{\mathrm{eff},0}(t')\mathrm{d}t'\right)^2}{2(\sigma_0^2+2Dt)}\right)}{\sqrt{2\pi}(\sigma_0 + \sqrt{2Dt})} \tag{45}$$

with $G_{\mathrm{eff},0}(t) = G - S\bar{\rho}(t)$ and the analytic expression $\bar{\rho}(t)$ from Eq. (26). Again, the transition from the domain $l/L \in \mathbb{R}$ of $\varrho(l,t)$ to $l \in [L, 2L]$ of the desired $\rho(l,t)$ is formally possible via Eq. (34). The resulting length distribution is shown in Fig. 2D of the main manuscript.

It is also possible to determine the stationary length distribution analytically from the condition of a constant length current J_l. To this end, we need to solve

$$\frac{\partial}{\partial l}\left(D\frac{\partial}{\partial l}h_\infty(l) + Sh_\infty(l)\bar{\rho}_\infty - Gh_\infty(l)\right) = -\frac{\partial J_l}{\partial l} = 0\,.$$

(46)

subject to the oblique boundary condition $h_\infty(L) = 2h_\infty(2L)$ deduced from Eq. (15). Defining

$$\alpha := (G - S\bar{\rho}_\infty)/D$$

(47)

we can explicitly write all possible stationary solutions of Eq. (46) in the form

$$h_\infty(l,\alpha) = \frac{\alpha\left(e^{\alpha\,(l-L)} + 1 - 2e^{\alpha\,L}\right)}{(1 - 2\alpha L)e^{\alpha\,L} - 1 + \alpha\,L}\,,$$

(48)

for $l \in [L, 2L]$ and $h_\infty(l,\alpha) = 0$ otherwise.

For the value $\alpha = -\ln 2$, our result (48) reduces to the pure exponential form $h_\infty(l) := h_\infty(l, -\ln 2)$ from Eq. (43), which is also recovered as the unique stationary result when numerically solving Eq. (22). This solution is distinguished from all other distributions $h_\infty(l,\alpha)$ for the following reasons. First, the stationary length current $J_l = 0$ vanishes. Second, it turns out that $h_\infty(l)$ is the only solution which is stable upon small fluctuations $\delta\bar{\rho}(t)$ of the average density. This can be understood from inserting $\bar{\rho}(t) = \bar{\rho}_\infty + \delta\bar{\rho}(t)$ into Eq. (22) which yields the linearized equation

$$\frac{\partial\rho(l,t)}{\partial t} = S\bar{\rho}_\infty\frac{\partial h_\infty(l,\alpha)}{\partial l}\delta\bar{\rho}(t)\,.$$

(49)

From this result we see that the dynamics tends to revert the perturbation in the density (since the slope of all length distribution is negative) but also induces fluctuations in the length distribution, unless $\partial h_\infty(l,\alpha)/\partial l \propto h_\infty(l,\alpha)$, which is only the case for $\alpha = -\ln 2$. This observation provides a good indication that this particular stationary solution will be approached. Third, $h_\infty(l)$ is the only distribution for which the density remains a differentiable function in l under translation through the boundary, which can be explicitly checked by constructing $\sum_{n=-\infty}^{\infty} 2^n h_\infty(l + nL, \alpha)$ similar to Eq. (34). Therefore, as also remarked in the previous sections, the initial condition $h_0(l) = h_\infty(l) = \frac{4\ln 2}{L}2^{-l/L}$ results in a uniform time evolution of $h(l,t)$ such that $\bar{\rho}(t)$ is given by Eq. (26), which has been determined from exactly this assumption (23) that the exponential form of $h(l,t)$ does not change over time.

Relatedly, we notice that, due to the form of $h(l,t)$, the effective elongation rate also depends on the fluctuations. Assuming the stationary distribution $h_\infty(l)$, as in the related growth equation, Eq. (24), we find the overall effective elongation rate

$$G_{\text{eff}}(t) := G + D\frac{\ln 2}{L} - S\bar{\rho}(t) = G_{\text{eff},0}(t) + D\frac{\ln 2}{L}$$

(50)

with an additional term compared to the effective drift velocity $G_{\text{eff},0}(t)$ used before in Eqs. (37) and Eq. (45). This means that, due to the asymmetry of $h_\infty(l)$, the faster growing bacteria make a stronger contribution than the slower growing ones, as the former divide earlier. When $h(l,t)$ is nonuniform, the generalized effective elongation rate

$$\tilde{G}_{\text{eff}}(l,t) := G + D\frac{\partial_l h(l,t)}{h(l,t)} - S\bar{\rho}(t)$$

(51)

even depends explicitly on the current length of the bacteria.

5. Fluctuation-driven growth

Finally, we consider the case of extreme fluctuations $D > 0$ while $G = S = 0$ in Eq. (22), which gives rise to

$$\frac{\partial\rho(l,t)}{\partial t} = D\frac{\partial^2\rho(l,t)}{\partial l^2}\,.$$

(52)

In this particular limit, our model predicts the particular stationary solution $h_\infty(l) = \frac{2}{L} - \frac{2l}{3L^2}$ which is the limit of Eq. (48) for $\alpha \to 0$. The formal solution for the dynamics of $\rho(l,t)$ is the same as obtained in the uniform regime, Eq. (39) but with $G = 0$.
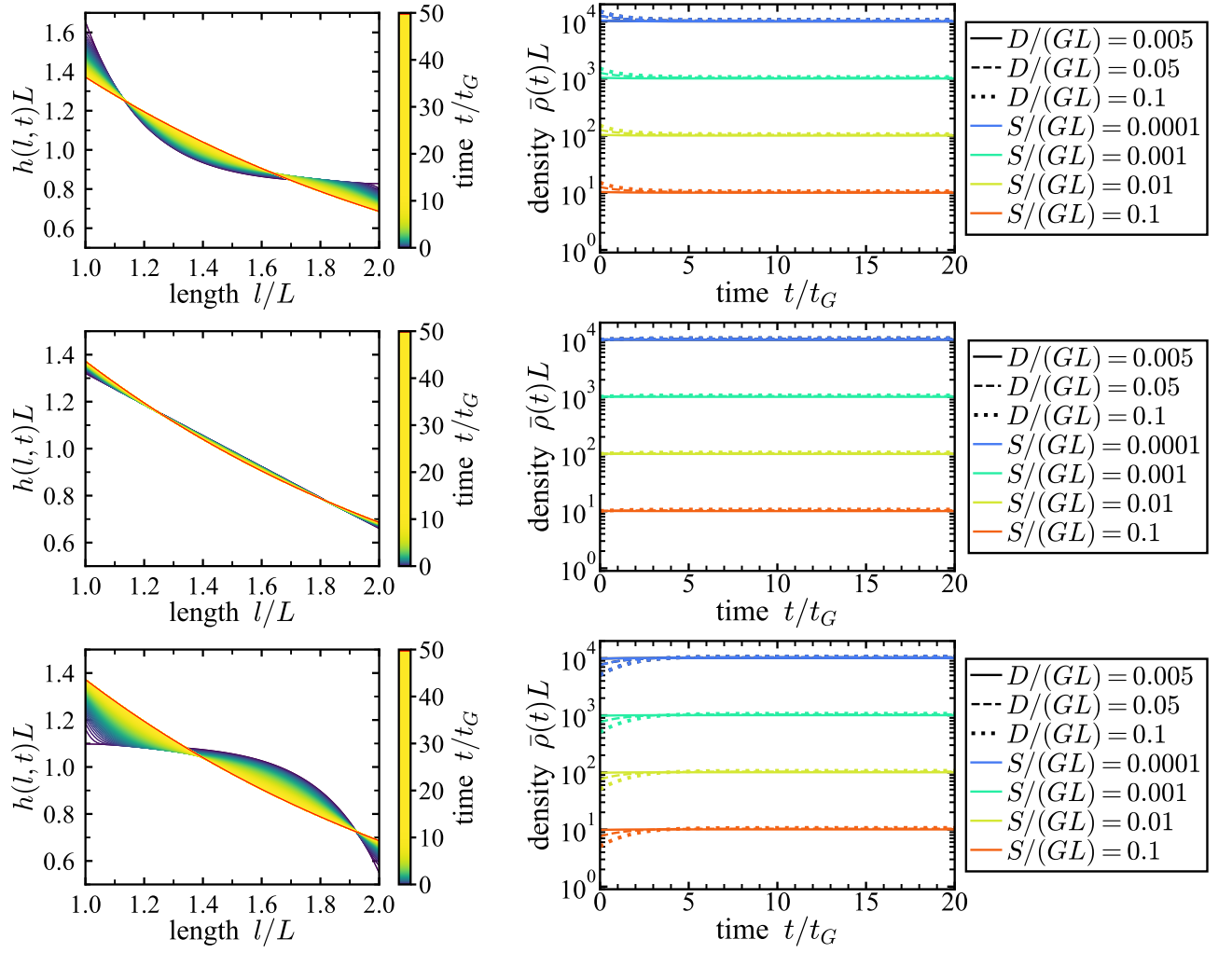
FIG. 5. Approach to the current-free stationary state given by Eqs. (48) and (47) with $\alpha = -\ln 2$ starting from different unstable solutions (48) with $\alpha = -5$ (top), $\alpha = 0$ (middle) and $\alpha = 5$ (bottom), choosing the initial density as $\bar{\rho}_0 = (G - D\alpha)/S$ consistently with Eq. (47). In each case, the left column shows the time evolution ($t_G := L/G$) of the length distribution $h(l, t)$ towards $h_\infty(l)$ (red) for $D = 5 \times 10^{-3} GL$ and $S = 10^{-4} GL$, while the right column depicts the change of the average density $\bar{\rho}(t)$ for various combination of parameters according to the legend.

C. Numerical evaluation

1. Numerical check for stability

As concluded from Eq. (49), we indeed find numerically that the stationary solutions in Eq. (48) with the parameter α from Eq. (47) are numerically unstable unless $\alpha = -\ln 2$. Figure 5 shows that from these initial conditions, the system evolves towards the unique current-free solution with $\alpha = -\ln 2$ and the average density adapts accordingly.

2. Refined DDFT model for cell division with directed boundary condition

In Sec. I B 1 we have introduced two variants of the coarse-grained DDFT with a length-resolved density. The formulation of DDFT based on the oblique periodic boundary condition (15) and the continuity equation (14) is convenient for making analytic progress. However, the variant in Eq. (12), which models cell division through source and sink terms, is more adjustable. It can be directly applied in the more general DDFT resolving positional and orientational degrees of freedom, cf. Eq. (11), and is also compatible with any kind of boundary condition. The latter point constitutes an advantage when the colony becomes denser and the dynamics are governed by mechano-self-
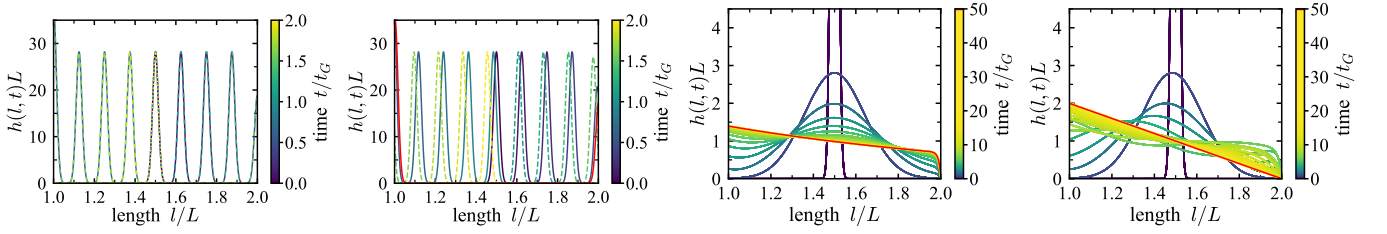
FIG. 6. Analogous length distribution to Fig. 2A-D of the main manuscript reconsidered here from evaluating the DDFT (53) with the current from Eq. (54) and the directed boundary condition from Eqs. (55) and (56). From the left to the right, the parameters are $S = 0$ and $D = 0$, $S = 10^{-2}G/\bar{\rho}_0$ and $D = 0$, $S = 0$ and $D = 10^{-2}GL$, as well as, $S = 10^{-2}G/\bar{\rho}_0$ and $D = 10^{-2}GL$.

regulation, such that it becomes important to understand what exactly happens at the boundary. In fact, mechano-self-regulation (and also fluctuations) can formally result in the shrinking of cells. If they were allowed to shrink over a periodic boundary from $l = L$ to $l = 2L$, the description would amount to two small cells with length L reuniting back to one large cell with length $2L$.

To this end, we use the description of cell division by source and sink terms to propose the refined DDFT model

$$\frac{\partial \rho(l,t)}{\partial t} = -\frac{\partial}{\partial l} J_l(l,t) + 2\delta(l - L)J_l\left(2L, t\right) - \delta(l - 2L)J_l\left(2L, t\right) \tag{53}$$

with $l \in [L, 2L]$ and the current

$$J_l(l,t) = -D\partial_l\rho(l,t) - S\rho(l,t)\bar{\rho}(t) + G\rho(l,t) \tag{54}$$

from Eq. (21). Instead of a periodic boundary condition, we here use at $l = L$ the no-flux boundary condition

$$D\partial_l\rho(l = L, t) \overset{!}{=} 0 \tag{55}$$

for the fluctuation term and at $l = 2L$ an absorbing wall, i.e.,

$$\rho(l > 2L, t) \overset{!}{=} 0 \,. \tag{56}$$

Now the cells can still grow over the boundary from $2L$ to L, but are stuck with their short elongation at $l \gtrsim L$ if they shrink. In this refined model, mechano-self-regulation results in a larger number of shorter cells, which is the dominant experimental aspect, but not in two short cells reuniting to form a single large cell. This behavior can only be recast by using source and sink terms. The directed boundary condition from Eqs. (55) and (56) can also be used for the general DDFT in Eq. (11).

3. Supplementary DDFT results with directed boundary condition

In Fig. 6 we show the DDFT results of the refined model for cell division, introduced in Sec. II C 2, for the same quantities and parameters as in Fig. 2 of the main manuscript, which shows the DDFT results, discussed in Sec. II B, modeling cell division by the oblique boundary condition.

Since the difference between the two boundary conditions only concerns the fluctuation term, the first two plots in Fig. 6 for $D = 0$ show the same behavior as Fig. 2A (oscillating growth) and Fig. 2B (retarded growth) of the main manuscript, respectively. The stationary length distribution in the third plot of Fig. 6 with $S = 0$ but $D > 0$ is no longer given by an exponential as for the uniform growth in Fig. 2C of the main manuscript, which is most apparent from the behavior for $l \approx 2L$. Finally, for $S > 0$ and $D > 0$, we observe a retarded and uniform growth, although the unique stationary length distribution decays linearly and thus differs from the form in Fig. 2D of the main manuscript.

III. LANGEVIN SIMULATIONS OF GROWING BACTERIAL COLONIES

A. Supplementary simulation methods

In the particle-based approach to modeling growing bacteria colonies, the cells are considered as rigid rods. Their positions $\boldsymbol{r}_i$, orientations θ_i and lengths l_i (of their long axis) evolve in time according to coupled Langevin equations. Here $i = 1, \ldots N$ is the cell index, where the total number $N(t)$ of bacteria may increase after each time step due to cell division. The short axis of each rod is kept fixed with length d_0.

The position $\boldsymbol{r}_i$ of rod i evolves according to

$$\frac{\mathrm{d}\boldsymbol{r}_i}{\mathrm{d}t} = \frac{1}{\gamma l_i} \sum_j \boldsymbol{F}_{ij}, \tag{57}$$

where γ is the friction coefficient and $\boldsymbol{F}_{ij}$ are steric forces stemming from the interactions with other rods. Further, the orientation of the rod is measured by the angle θ_i with respect to the x-axis in a Cartesian coordinate system. The dynamics of the angles are given by

$$\frac{\mathrm{d}\theta_i}{\mathrm{d}t} = \frac{12}{\gamma l_i^3} \sum_j \left(\boldsymbol{r}_{ij} \times \boldsymbol{F}_{ij} \right) \cdot \boldsymbol{e}_z, \tag{58}$$

where $\boldsymbol{r}_{ij} = \boldsymbol{r}_i - \boldsymbol{r}_j$ is the distance vector between particles i and j and $\boldsymbol{e}_z$ is the vector perpendicular to the rods' plane of motion. The forces between rods are calculated by a Hertzian repulsion

$$\boldsymbol{F}_{ij} = F_0 d_0^{1/2} h_{ij}^{3/2} \boldsymbol{n}_{ij}, \tag{59}$$

where h_{ij} is the overlap of rod i and j, F_0 is the strength of the force, and $\boldsymbol{n}_{ij}$ is the vector normal to the closest point of contact of the particles.

In the same spirit, we now allow the length of a rod i to evolve as

$$\frac{\mathrm{d}l_i}{\mathrm{d}t} = G + \sqrt{2D}\xi_i + \tilde{S} \sum_j h_{ij}^{3/2} \tag{60}$$

with the elongation rate G, a white noise ξ_i of unit variance accounting for fluctuations of magnitude D and mechanical self-regulation mediated by the overlap between particles h_{ij}. The parameter $\tilde{S}$ quantifies the strength of this mechano-self-regulation, where we have absorbed the other parameters from Eq. (59). When the length l_i of a cell exceeds the value $2L$ after a certain time step, it is reset to $l_i = L$, where L is the length-at-birth. Then, a second cell with a new particle label and the same length L is introduced and the total cell count N is increased accordingly. In the course of this cell division the positions of the two daughter are shifted from the rods original position by $L/2$ along the direction of the rod.

In the main text, the repulsion strength is fixed as $F_0 = 10^6 G/(\gamma L)$ and the short axis of each rod as $d_0 = L/8$. The data presented in our plots are averaged over five simulation runs.

B. Supplementary simulation data

The length distributions associated with the four snapshots in Fig. 3A-D of the main manuscript are shown in Fig. 7.
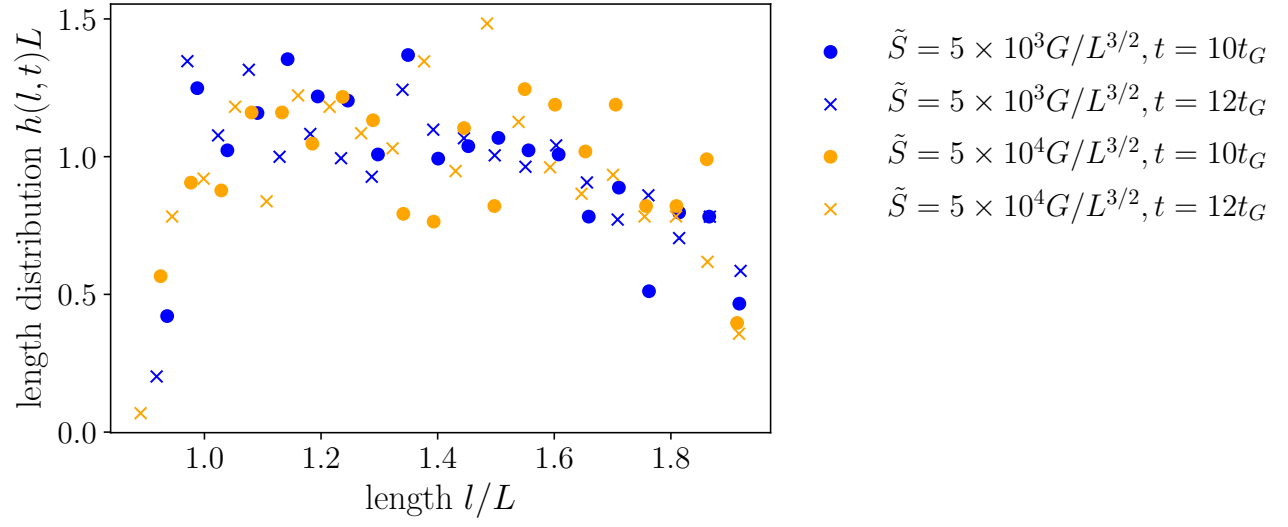
FIG. 7. Length distributions of four different colonies.

IV.   EXPERIMENTS ON GROWING BACTERIAL COLONIES

A.   Supplementary experimental methods

1.   Cell culture protocol for bacterial species

We use non-motile strains of *E. Coli* bacteria, NCM3722 delta-motA, growing at 30°C. All experiments have been performed for a minimum of two distinct biological replicates. As a first step, the cells where streaked on standard agar plates replete with Lysogeny broth (LB). The plated cells were grown for a day, after which isolated cell colonies were identified, and scraped using a microbiological loop. The growth temperature of the cell culture incubator as well as incubated attached to the imaging microscope was set to 30°C. The scraped cells were then transferred to a liquid LB media, and allowed to divide in a shaker for ∼12h. Thereafter, the culture was sampled at regular intervals in order to track the cell growth over time, using the optical density (OD) measurement technique. After nearly 12 hours of liquid culture growth, the cells were transferred into fresh LB media, at a 1:1000 ratio of cell to fresh media, and grown for ∼2h, before they were introduced on the specially designed substrates (see next section). Additional details on the cell culturing protocols and control experiments can be found in Ref. 19.

2.   Fabrication of microscale confinements for studying bacterial growth

The single cell-to-colony dynamics were observed using time-lapse microscopy on a millimeter thick layer of agarose gel. The gel was first uniformly mixed with the LB medium, making it a nutrient-rich substrate. This nutrient-replete layer was sandwiched between two glass slides and a 2mm thick Gene Frame (spacer) was used to enclose the glass-agarose system. A time-lapse phase-contrast microscopy, with feedback controlled focussing technique, imaged the growth of the sessile colonies using an inverted imaging mode. The sample, placed ont he microscope stage, was enclosed within a thermally insulated temperature-controlled incubator (Pecon), which could be regulated precisely to set the temperature, and monitored temperature at the sample with a resolution of 0.1°C. Please refer to Ref. 19 for further details of the microscale set up and the imaging configuration.

3.   Time-lapse phase-contrast imaging

The growth of a single bacterium (or two initial cells, in some cases) into colonies is imaged while maintaining the growth temperature of 30°C within the microscope environment. Single bacterium acting as monoclonar nucleating sites expand horizontally ont he nutrient-rich agarose layers. Initially, the colony grows in two dimensions as a *bacterial monolayer* over multiple generations, subsequently penetrating into the third dimension. We visualize the colony growth over the entire time span (lasting up to 15 h to 18 h, depending on the growth conditions) using time-lapse phase-contrast microscopy. For the current work, we focus primarily on the horizontal spreading of the colony, and analyze the data till the transition to the multilayer structure sets off. Images were acquired using a Hamamatsu ORCA-Flash Camera ($1\mu m = 10.55$ pixels) that was coupled to an inverted microscope (Olympus CellSense LS-IXplore). We use a 60X oil objective, and in some cases 100X oil objectives to zoom into specific regions of the growing colonies. Overall, this gave a minimum resolution of $0.11\mu m$. Each experiment lasted typically 15h to 18h, allowing us to capture the mono-to-multilayer configurations, and the structure and dynamics of multilayer colonies. Prior to image acquisition, multiple locations on the agarose surface (where a single bacterium or up to two cells were present) were identified and recorded, allowing us to additionally extract technical replicates from the same sample. The microscope was automated to scan these pre-recorded coordinates and to capture the images of the gradually increasing colonies after every 5 minutes while maintaining the focus across all the colonies captured. We extracted the cell dimensions (width and length), position (centroid) and the orientation of each bacteria from the phase-contrast images using the combination of open-source packages of Ilastik [83] and ImageJ as well as MATLAB (MathWorks), as detailed in Sec. IV A 4.

4.   Image analysis

The counting process consists of cell segmentation followed by counting the number of individual entities. Cell segmentation is performed using a combination of Ilastik-MATLAB coding that helped to extract the bacterial length and orientation in the colony for each time frame of the bacterial colony growth. The process is continued till

the colony encounters the mono-to-multilayer transition, since after this event the image contrast and focus gets limited for subsequent segmentation. However, further analysis can be carried out using particle image velocimetry algorithms (see Ref. 19). Raw images are initially pre-processed using by a combination of background subtraction and preliminary thresholding. The pre-processed image is then trained using Ilastik for accurate segmentation (see Ref. 83). The training process involves iteration until a reasonably satisfactory extraction is obtained. A labeled image is extracted from the segmentation process and identified in MATLAB. A bacillus-shaped water-shedding technique is performed to separate out joint bacterial cells. Finally, these individual entities (segmented cells) are colored or outlined for counting and analysis. Further relevant details on the image analysis protocols can be found in Ref. 19.

B. Supplementary experimental data

1. Cell length statistics for replicate 1

For the cell size statistics of replicate 1 analyzed in Figs. 1 and 4 of the main manuscript, please refer to Table I.

2. Cell length statistics for replicate 2

For the cell size statistics of replicate 2 analyzed in Fig. 4 of the main manuscript, please refer to Table II.

TABLE I. Cell length statistics for replicate 1

Time $(t$, min)	Length $(\bar{l}, \mu$m)	SD $(\mu$m)	Variance (μm^2)	Variance$/\langle\bar{l}\rangle^2$ $(\langle\bar{l}\rangle = 3.83\ \mu$m)
0	3.36	0.96	0.9216	0.0628
5	3.19	0.92	0.8464	0.0577
10	3.42	0.86	0.7396	0.0504
15	2.87	0.76	0.5776	0.0394
20	3.09	0.84	0.7056	0.0481
25	2.91	0.33	0.1089	0.0074
30	2.86	0.35	0.1225	0.0084
40	4.11	0.56	0.3136	0.0214
50	3.84	0.45	0.2025	0.0138
60	3.76	1.08	1.1664	0.0795
75	4.34	1.24	1.5376	0.1048
85	3.95	0.69	0.4761	0.0325
100	4.42	0.44	0.1936	0.0132
115	4.95	1.18	1.3924	0.0949
125	3.76	1.28	1.6384	0.1117
140	4.87	1.32	1.7424	0.1188
150	5.15	0.92	0.8464	0.0577
160	4.88	1.61	2.5921	0.1767
175	4.00	1.21	1.1464	0.0998
185	4.83	1.08	1.1664	0.0795
200	4.42	1.30	1.6900	0.1152
215	4.19	1.33	1.7689	0.1206
225	4.50	1.44	2.0736	0.1414
235	4.62	1.56	2.4336	0.1659
250	4.89	0.92	0.8464	0.0577
270	4.71	1.41	1.9881	0.1355
280	4.28	1.37	1.8769	0.1280
290	4.36	1.36	1.8496	0.1261
300	4.76	1.36	1.8496	0.1261
310	4.72	1.41	1.9981	0.1355
320	4.51	1.37	1.8769	0.1280
330	4.02	1.21	1.4641	0.0998
340	3.88	1.04	1.0816	0.0737
350	3.23	0.98	0.9604	0.0655
360	3.58	1.04	1.0816	0.0737
370	3.38	1.05	1.1025	0.0752
380	3.29	0.94	0.8836	0.0602
390	3.13	0.93	0.8649	0.0590
400	3.11	0.92	0.8464	0.0577
410	2.90	0.90	0.8100	0.0552
420	3.21	1.01	1.0201	0.0695
435	2.98	0.86	0.7396	0.0504
455	2.74	0.84	0.7056	0.0481
465	2.71	0.81	0.6561	0.0447

TABLE II. Cell length statistics for replicate 2

Time (t, min)	Length ($\bar{l}$, μm)	SD (μm)	Variance (μm^2)	Variance/$\langle\bar{l}\rangle^2$ ($\langle\bar{l}\rangle = 3.88$ μm)
0	4.35	0.03	0.0009	0.0001
5	4.79	0.08	0.0064	0.0004
10	3.31	1.65	2.7225	0.1808
15	3.43	1.69	2.8561	0.1897
20	2.70	0.21	0.0441	0.0029
25	2.75	0.12	0.0144	0.0010
30	2.93	0.19	0.0361	0.0024
40	3.31	0.15	0.0225	0.0015
50	4.04	0.35	0.1225	0.0081
60	4.63	0.44	0.1936	0.0129
75	3.96	1.18	1.3924	0.0925
85	3.35	0.32	0.1024	0.0068
100	4.67	0.51	0.2601	0.0173
115	5.76	0.65	0.4225	0.0281
125	3.36	0.56	0.3136	0.0208
140	4.55	1.02	1.0404	0.0691
150	4.91	1.06	1.1236	0.0746
160	4.14	1.37	1.8769	0.1247
175	4.02	0.76	0.5776	0.0384
185	4.66	0.92	0.8464	0.0562
200	4.18	1.82	3.3124	0.2200
215	4.22	1.56	2.4336	0.1617
225	4.62	1.24	1.5376	0.1021
235	5.24	1.37	1.8769	0.1247
250	3.94	1.25	1.5625	0.1038
270	4.83	1.16	1.3456	0.0894
285	4.10	1.36	1.8496	0.1229
300	4.14	0.96	0.9216	0.0612
335	4.00	1.08	1.1664	0.0775
350	3.84	1.06	1.1236	0.0746
385	3.22	0.85	0.7225	0.0480
400	3.03	0.96	0.9216	0.0612
415	2.71	0.80	0.6400	0.0425
425	2.90	0.78	0.6084	0.0404
435	2.97	0.80	0.6400	0.0425
440	3.01	0.84	0.7056	0.0469
445	2.99	0.84	0.7056	0.0469